UNIVERSITYOF BIRMINGHAM

University of Birmingham Research at Birmingham

Endochondral bone in an Early Devonian 'placoderm' from Mongolia

Brazeau, Martin D.; Giles, Sam; Dearden, Richard P.; Jerve, Anna; Ariunchimeg, Ya.; Zorig, E.; Sansom, Robert; Guillerme, Thomas; Castiello, Marco

1   **Endochondral bone in an Early Devonian 'placoderm' from Mongolia**

2

3   Martin D. Brazeau[1,2]*, Sam Giles [2,3,4], Richard P. Dearden[1,5], Anna Jerve[1,6], Y.A.

4   Ariunchimeg[7], E. Zorig[8], Robert Sansom[9], Thomas Guillerme[10], Marco Castiello[1]

5

6   [1] *Department of Life Sciences, Imperial College London, Silwood Park Campus, Buckhurst*

7   *Rd, Ascot, SL5 7PY, UK;*

8   [2] *Department of Earth Sciences, Natural History Museum, Cromwell Road, London SW7*

9   *5BD, UK;*

10   [3] *School of Geography, Earth and Environmental Sciences, University of Birmingham,*

11   *Birmingham, UK;*

12   [4] *Department of Earth Sciences, University of Oxford, South Parks Road, Oxford, OX1 3AN,*

13   *UK;*

14   [5] *CR2P Centre de Recherche en Paléontologie – Paris, Muséum national d'Histoire*

15   *naturelle, Sorbonne Universités, CNRS, CP 38, 57 Rue Cuvier, 75231, Paris, Cedex 05,*

16   *France*

17   [6] *Department of Organismal Biology, Subdepartment of Evolution and Development,*

18   *Uppsala University, Norbyvägen 18A, 752 36 Uppsala, Sweden;*

19   [7] *Natural History Museum, P.O. Box 46/52, Ulaanbaatar 1420, Mongolia*

20   [8] *Institute of Paleontology, Mongolian Academy of Science, P.O. Box 46/650, S. Danzan*

21   *Street 3/1, Chingeltei District. Ulaanbaatar 15160, Mongolia;*

22   [9] *School of Earth and Environmental Sciences, University of Manchester, Manchester M13*

23   *9PT, UK;*

24   [10] *Department of Animal and Plant Sciences, The University of Sheffield, Sheffield S10 2TN,*

25   *UK;*

26

27   * Author for correspondence.

28 **Endochondral bone is the main internal skeletal tissue of nearly all osteichthyans—the**

29 **group comprising more than 60,000 living species of bony fishes and tetrapods.**

30 **Chondrichthyans (sharks and their kin) are the living sister group of osteichthyans and**

31 **have cartilaginous endoskeletons, long considered the ancestral condition for all jawed**

32 **vertebrates (gnathostomes). The absence of bone in modern jawless fishes and the**

33 **absence of endochondral ossification in early fossil gnathostomes appears to lend**

34 **support to this conclusion. Here we report the discovery of extensive endochondral bone**

35 **in *Minjinia turgenensis*, a new genus and species of 'placoderm'-like fish from the Early**

36 **Devonian (Pragian) of western Mongolia described using x-ray computed**

37 **microtomography (XR-μCT). The fossil consists of a partial skull roof and braincase**

38 **with anatomical details providing strong evidence of placement in the gnathostome stem**

39 **group. However, its endochondral space is filled with an extensive network of fine**

40 **trabeculae resembling the endochondral bone of osteichthyans. Phylogenetic analyses**

41 **place this new taxon as a proximate sister group of the gnathostome crown. These**

42 **results provide direct support for theories of generalised bone loss in chondrichthyans.**

43 **Furthermore, they revive theories of a phylogenetically deeper origin of endochondral**

44 **bone and its absence in chondrichthyans as a secondary condition.**

45

46 The vertebrate skeleton comprises two main systems: the exoskeleton (external achondral

47 dermal bones) and endoskeleton (internal chondral bones and cartilages, as well as some

48 intramembranous bones)[1]. An ossified exoskeleton evolved at least 450 million years ago in

49 jawless stem gnathostomes[2,3], but the endoskeleton in these taxa is not endochondrally

50 ossified. Endochondral bone, in which the cartilaginous endoskeletal precursor is invaded by

51 and eventually replaced by bone, is widely considered an osteichthyan apomorphy[3-7] and

52 such a reliable identifying character gives the group its name. Extant chondrichthyans lack

53   dermal bone and possess a mainly cartilaginous endoskeleton enveloped by a structurally

54   diverse range of tessellate calcified cartilage[8]. Outgroups of the gnathostome crown also lack

55   endochondral ossification. Galeaspids surround their cartilaginous skeleton in globular

56   calcified cartilage{NianZhong:2005tj}, while osteostracan and 'placoderm' endoskeletons

57   were sheathed in perichondral bone[3]. Consequently, the last common ancestor of jawed

58   vertebrates was long thought to have been perichondrally ossified, but lacking endochondral

59   ossification[3].

60   In this paper, we describe a new genus and species of 'placoderm' from the Early

61   Devonian of western Mongolia. Although Mongolia is known for some of the geologically

62   oldest putative gnathostome fossils (isolated chondrichthyan-like scales [9-12]), it remains a

63   poorly sampled region of the world with respect to early vertebrates. 'Placoderms' were until

64   now known from only a single fragmentary occurrence[13] in the early Middle Devonian

65   (Eifelian). Our new data highlight the importance of Mongolia as a key region for studies of

66   early gnathostome evolution. We describe a braincase and partial skull roof representing the

67   first substantial body fossil of an early gnathostome from Mongolia and displaying an

68   unexpected occurrence of endochondral bone analysed using XR-µCT. We conducted

69   phylogenetic analyses to reconstruct the evolutionary relationships of this new taxon. To

70   explore the evolutionary history of endochondral bone in light of this new discovery, we used

71   parsimony and maximum likelihood ancestral states reconstruction. Finally, we discuss these

72   results in the context of earlier statements about endochondral bone in non-osteichthyans,

73   new developments in understanding the complexity and diversity of chondrichthyan

74   endoskeletal tissues, and current uncertainties about early gnathostome phylogenetic

75   relationships.

76

77   **Systematic palaeontology**

78   Gnathostomata Gegenbaur, 1874[14]

79   *Minjinia turgenensis* gen. et sp. nov.

80

81 **Etymology.** Generic name honours the memory of Chuluun Minjin for his extensive

82 contributions to the Palaeozoic stratigraphy of Mongolia, his enthusiastic support of this

83 work, and introducing us to the Yamaat River locality. Specific name recognises the

84 provenance of the fossil from the Turgen region, Uvs aimag of western Mongolia.

85

86 **Holotype.** Institute of Paleontology, Mongolian Academy of Sciences MPC-FH100/9.1, a

87 partial braincase and skull roof.

88

89 **Type locality.** Turgen Strictly Protected Area, Uvs province, western Mongolia; near the top

90 of the stratigraphic sequence that occurs between the Tsagaan-Salaat and Yamaat Rivers.

91

92 **Formation and age.** Upper part of Tsagaansalaat Formation, Pragian (Early Devonian) [15,16].

93

94 **Diagnosis.** 'Placoderm'-grade stem gnathostome with endochondral bone, deep epaxial

95 muscle cavities flanking a slender occipital ridge, and the following possible autapomorphies:

96 dermal bones covered in sparsely placed tubercles, penultimate spino-occipital nerve canal

97 substantially larger in diameter than others.

98

99 **Description**

100 MPC-FH100/9.1 consists of a partial braincase and skull roof (Fig. 1). The skull roof is

101 ornamented with sparsely distributed finely ridged tubercles resembling those of the Siberian

102 'placoderm' *Dolganosteus*[17]; the tubercles become more broadly separated towards the

103   midline of the skull. They are distinct from those of *Dolganosteus* in that towards the midline

104   of the skull roof, the tubercles are larger and more pointed. The specimen shows signs of

105   extensive post-mortem transport, with angles of the braincase worn off and much of the skull

106   roof and some of the braincase preserved as a mould. Individual skull roof ossifications

107   cannot be identified, although this may be due to the dominantly mouldic preservation. There

108   appears to have been a prominent nuchal plate eminence comparable to certain

109   acanthothoracids such as *Romundina*[18] and *Arabosteus*[19].

110

111   **Endoskeletal tissue.** The braincase of MPC-FH100/9.1 is well ossified, comprising an

112   external bony sheath filled with an extensive matrix of spongy tissue (Fig. 2a-b; Extended

113   Data Fig. 1; Supplementary Video 1). The trabecles forming this tissue are irregular and

114   branching, less than 1 mm thick and often curved, and resemble most closely the

115   endochondral tissue of osteichthyans (Fig. 2c-d; Supplementary Video 2). As such, we

116   interpret this as endochondral bone. Notably, this is found in all preserved regions of the

117   braincase, in contrast to the isolated trabeculae previously identified as endochondral bone in

118   *Boreaspis*[20] and *Bothriolepis*[21]. The margins of the braincase, the endocranial walls, and the

119   boundaries of nerve and blood canals, are formed from a thicker tissue which we interpret as

120   perichondral bone. This suggests that the endoskeleton of *Minjinia* comprises osteichthyan-

121   like endochondral bone, with an ossified perichondrium. To address the possible alternative

122   explanation that it is an aberrant instance of calcified cartilage, we compared the structure of

123   this tissue with rarely-preserved mineralized cartilage in the stem chondrichthyan

124   *Diplacanthus crassismus* (National Museums of Scotland specimen NMS 1891.92.334; Fig.

125   2e-f) observed using synchrotron tomography. The cancellae within the endochondral tissue

126   of *Minjinia* are irregular, with a diameter of approximately 1-2 mm. This tissue is distinctly

127 unlike the calcified cartilage of *Diplacanthus* in appearance, which consists of a densely

128 packed matrix of irregularly stacked chondrons between 20-60 μm in diameter.

129

130 **Neurocranium.** The braincase is preserved from the level of the right posterior orbital wall

131 to the posterior end of the occipital ridge. Occipital glenoid condyles are not preserved, but

132 much of the rest of the broad, flat parachordal region is present, separated by a midline

133 groove that accommodated a relatively narrow notochordal tunnel. An asymmetric transverse

134 fissure spans the basicranial surface at about mid-length of the preserved portion. It appears

135 to demarcate the anterior margin of the parachordal plates and may correspond to the ventral

136 cranial fissure of crown-group gnathostomes. However, unlike in crown gnathostomes, it is

137 traversed by a substantial anterior extension of the cranial notochord. The courses of the

138 lateral dorsal aortae are marked by a pair of sulci on the lateral margins of the parachordal

139 plates, though only a short part of the canal is preserved on the right side of the specimen. A

140 narrow, shallow sulcus for the efferent hyoid artery is present on the preserved right side of

141 the specimen, immediately behind the level of the orbit (Fig. 1a).

142   The lateral surface of the braincase is preserved on the right side as a mouldic

143 impression in the matrix (Fig. 1). A sharply demarcated hyoid fossa is present on the lateral

144 wall of the otic region (Fig. 1). Posterior to this, a stout but pronounced vagal process with a

145 pair of rounded eminences likely corresponds to the branchial arch articulations. There is no

146 evidence for a pair of anterior and posterior divisions to the vagal process, which are

147 typically seen in other 'placoderms'. A well-developed 'placoderm'-like craniospinal

148 process is absent; its homologous position is instead covered in perichondral bone and

149 marked by a low ridge (Fig. 1).

150   In posterior view, a tall, narrow median occipital ridge is evident and resembles the

151 morphology of *Romundina*[22] and *Arabosteus*[19]. Similar to these taxa, the median otic ridge is

152 flanked by two large occipital fossae for the epaxial musculature. The notochordal tunnel is

153 approximately the same size as or smaller than the foramen magnum, as in 'placoderms' and

154 in contrast with crown-group gnathostomes. A metotic fissure is absent.

155

156 **Endocast.** A partial cranial endocast is preserved, consisting of the hindbrain cavity, partial

157 midbrain cavity, labyrinth cavities, and posteromedial corner of the orbital region. The two

158 primary trunk canals of the trigeminal nerve (N.V$_1$ and N.V$_{2,3}$) are preserved (Fig. 3). The

159 acoustic (N.VIII) and facial nerve (N.VII) canals share a common trunk canal behind the

160 trigeminal nerves, as in many other 'placoderms' [22-25]. The facial nerve canal branches into

161 palatal and hyomandibular branches between the saccular chamber and rear orbit wall (Fig. 3;

162 Extended Data Fig. 2), indicating this division was internal (deep) to the otic process. The

163 supraophthalmic branch opens into the rear wall of the orbit and part of its supraorbital

164 course is preserved (Fig. 3; Extended Data Fig. 2). A slender branch extends below the

165 labyrinth and divides into palatine and hyomandibular branches (Fig 3; Extended Data Fig.

166 2). As in other 'placoderm'-grade taxa, the vagus nerve (N. X) trunk canal is very large in

167 diameter and exits from immediately behind the labyrinth cavity (Fig. 3). The spino-occipital

168 region resembles other 'placoderms' in being extended. At least four spino-occipital nerve

169 canals are present in a linear series, and the penultimate canal is largest in diameter (Fig. 3).

170 Intercalating these is a network of occipital artery canals branching from the dorsal aortae.

171 The skeletal labyrinth is not complete on either side of the specimen, but can mostly

172 be reconstructed according to the assumption of bilateral symmetry. The most significant

173 feature is that the labyrinth and endolymphatic cavity are joined to the main endocavity

174 chamber (Fig. 3). This is a striking contrast to other 'placoderms' and closely resembles

175 crown-group gnathostomes[26]. The endolymphatic canals are elongate and tubular, extending

176 posterolaterally to reach the skull roof, though external openings cannot be clearly identified.

177   The anterior semi-circular canal follows the saccular cavity closely as in petalichthyids[27](Fig.

178   3). However, the horizontal and posterior canals appear to extend well away from the

179   saccular chamber (Fig. 3). The dorsal junctions of the anterior and posterior canals are joined

180   in a crus commune, as in *Romundina*[22] and *Jagorina*[23]. A sinus superior is absent.

181

182   **Phylogenetic analyses**

183   We conducted phylogenetic analyses under four different protocols: equal weights

184   parsimony, implied weights parsimony, an unpartitioned Bayesian analysis, and a Bayesian

185   analysis with characters partitioned by fit determined under implied weights parsimony[28] (see

186   Extended Data Figs. 3-6). All phylogenetic analyses consistently place *Minjinia* as a stem-

187   group gnathostome, proximate to the gnathostome crown (Fig. 4, Extended Data Figs 3, 4).

188   *Minjinia* is recovered in a position crownward of arthrodires but outside of a grade consisting

189   of *Entelognathus*, *Ramirosuarezia*, and *Janusiscus*. Under implied weights parsimony, these

190   three taxa move onto the osteichthyan stem and *Minjinia* is placed as the immediate sister

191   taxon of the gnathostome crown. Under parsimony, the crownward position of *Minjinia* is

192   unambiguously supported by the skeletal labyrinth and endolymphatic duct being confluent

193   with the main cranial cavity[26] (Supplementary Information). In common with arthrodires and

194   the gnathostome crown[29], *Minjinia* possesses a division of the facial nerve(Fig. 3; Extended

195   Data Fig. 2) deep to the transverse otic process. However, *Minjinia* is excluded from the

196   gnathostome crown group due to the absences of a metotic fissure and a posterior dorsal

197   fontanelle, and presence of broad, flat parachordal plates expanded behind the saccular cavity

198   (Fig. 3, Supplementary Information).

199   We undertook ancestral states reconstructions to assess the evolutionary history of

200   endochondral bone (Fig. 4; Extended Data Figs. 5 & 6; Supplementary Information).

201   Interestingly, parsimony analysis fails to recover secondary homology of this trait between

202   *Minjinia* and osteichthyans. The crownward placement of *Minjinia* is, in fact, based on

203   independent evidence relating to anatomical features of the braincase and endocast. However,

204   the resolution becomes ambiguous if missing data in either *Entelognathus* or *Ramirosuarezia*

205   are resolved as having endochondral bone. The reconstruction becomes similarly ambiguous

206   if *Janusiscus* is moved a single branch (requiring only two additional steps) onto the

207   chondrichthyan stem. The strict precision of parsimony reconstructions makes it insensitive

208   to this underlying uncertainty. To explore this, we used likelihood reconstructions and

209   compared the ancestral state reconstructions under equal rates (ER) and all rates different

210   (ARD) variants of the Mkv model on branch-length-rescaled parsimony trees and Bayesian

211   trees. Both models show substantial non-zero marginal likelihoods if endochondral bone is

212   assumed present in the common node of *Minjinia* and Osteichthyes, with ARD strongly

213   favouring its presence (0.33 for ER; 0.81 for ARD; Fig. 3, Table 1, Extended Data Figs. 5, 6,

214   Supplementary Table 1). Under the ARD model, there is nearly equivocal support for

215   presence or absence of endochondral bone at the gnathostome crown node (Table 1). The

216   ARD model shows the best fit for endochondral bone (likelihood ratios 4.75 for parsimony [p

217   = 0.029] and 5.26 for Bayesian, [p = 0.022]) (Table 1, Supplementary Table 1), favouring

218   repeated losses of this tissue over multiple gains (see Discussion).

219

220   **Discussion**

221   *Minjinia turgenensis* presents an unexpected discovery of extensive endochondral bone in a

222   'placoderm'-grade fish, with repercussions for the phylogenetic origin of this tissue and the

223   problem of early gnathostome relationships more generally. The prevailing hypothesis has

224   been that endochondral bone is an osteichthyan apomorphy[3,7,29]. However, recent discoveries

225   have cast doubt on this assertion. The recognition that dermal bone is secondarily lost in

226   chondrichthyans[30,31] (Fig. 4) is consonant with prior knowledge of the loss of perichondral

227 bone in this same lineage[32]. Taken together, this has revived uncertainty about the true

228 phylogenetic timing of the origin of endochondral ossification[33]. *Minjinia* provides direct

229 corroboration for a more ancient origin.

230   *Minjinia* does not represent the first report of endochondral bone outside of

231 Osteichthyes. However, it is by far the most extensive and unequivocal example and raises

232 explicit questions in light of the proximity of *Minjinia* to the gnathostome crown (Fig. 4;

233 Extended Data Figs. 3, 4). Isolated examples of trabecular endoskeletal bone have historically

234 been reported in boreaspid osteostracans[20,34], a rhenanid[35], arthrodires[36], a ptyctodont[37], and a

235 petalichthyid[38,39]. However, these reports are nearly all unillustrated statements; they have all

236 been considered tenuous[3] or dismissed as misidentifications[5]. In line with these assessments,

237 we found no evidence of endochondral bone in material of *Buchanosteus* held in the Natural

238 History Museum, London, or indeed in any other 'placoderms' we have examined. The

239 *Epipetalichthys* holotype (Museum für Naturkunde, Berlin specimen MB.f.132.1-3) shows an

240 apparently spongiose infilling in the anterior region of the braincase, but the identity of this

241 structure, or even whether it is biological, cannot be determined. The *Epipetalichthys* tissue

242 figured by Stensiö[38] was very superficial, and possibly represents the retreat of perichondral

243 bone deposited during cartilage growth[39]. Most recently, trabeculae in supposed endoskeletal

244 pelvic bones of *Bothriolepis* have been termed endochondral bone[21], although the small scale

245 of these is in line with 'superficial' perichondral trabeculae seen elsewhere[38]. The reported

246 examples in boreaspid osteostracans have also been dismissed by later authors[3,5]. Although

247 they warrant further study, their tissue structures are unlikely to be homologous to

248 osteichthyans owing to their phylogenetic remoteness and nested position in the

249 Osteostraci[40].

250   Among chondrichthyans, endochondral bone has been mentioned in 'acanthodians'[3,41]

251 and superficial bone-like tissues have been reported in the skeletons of extant

chondrichthyans. We are unable to substantiate statements about acanthodians: no authors

have cited primary sources or specimens. One possible source is Watson's[42] description of

"massive ossification" of the endoskeleton of *Diplacanthus*. However, our synchrotron data

of this same specimen (Fig. 2) shows that this tissue is undoubtably calcified cartilage. Some

authors have speculated that the superficial mineralised tissue in the jaws of acanthodians or

chondrichthyans may have developed in an endochondral position[39]. Histological studies

show that endoskeletal mineralization in the jaws of acanthodians is globular calcification

and occasionally 'sub-tessellate'[8,43]. Recent comparative histology and development in extant

chondrichthyans has shown the presence of an extensive canalicular network in the tesserae[44]

and a trabecular tesseral network in some vertebral elements[45], both resembling bone.

Whether these represent homologues of osteichthyan examples remains open to debate;

future works could employ synchrotron microtomography of stem-chondrichthyan cartilages

to address these questions.

Does endochondral bone have a deep origin within the gnathostome stem group? This

would imply repeated losses of this tissue. We do find statistical support for this hypothesis

(Fig. 4, Table 1, Extended Data Figs. 5, 6, Supplementary Table 1), and the model is well

justified on prior phylogenetic and biological grounds. Endochondral bone has long been

known to be inconsistently developed across 'primitive' bony fishes: incomplete,

polymorphic, or entirely absent ossification of the endoskeleton is known in both Palaeozoic

actinopterygians[41,46,47] and sarcopterygians{Cloutier:wm}, as well as more recent taxa[48]. The

frequent absence of endochondral bone in osteichthyans is considered secondary, and other

controlling factors such as body size, maturity, mechanical stress, and buoyancy can

determine its degree of development[1]. Our findings are also in agreement with studies

establishing a genetic basis for secondary loss of all bone types within chondrichthyans[49-51],

276 with the failure to produce endochondral bone likely representing arrested development of

277 chondrocytes as opposed to a primary lack of ability[52].

278   Another confounding factor in this question is the problem of 'placoderm'

279 relationships. Although currently resolved in most analyses as a deeply pectinate grade along

280 the gnathostome stem (Fig. 4), the backbone of this arrangement has poor statistical support,

281 even in the present analysis (Extended Data Figs. 3). There is a lack of consistency in the

282 arrangement of plesia and Bayesian tip-dating methods have even recovered a monophyletic

283 Placodermi[53]. *Minjinia* itself highlights this uncertainty, given its highly unexpected character

284 combinations. Notwithstanding its endochondral bone and crown-gnathostome-like inner ear

285 structure, it resembles 'acanthothoracids'—the 'placoderms' widely considered among the

286 most removed from the gnathostome crown (i.e. most 'primitive'): it possesses deep epaxial

287 fossae either side of a prominent occipital ridge and a nuchal eminence otherwise seen only

288 in acanthothoracids such as *Romundina*[18] and *Arabosteus*[19]. This apparent character conflict

289 could perhaps be more easily reconciled with a more coherent (though not necessarily

290 monophyletic) 'placoderm' assemblage. Indeed, the highly pectinate structure of the

291 'placoderm' grade seems symptomatic of an overemphasis on characters and taxa resembling

292 the crown group, thereby undersampling characters that could stabilise a clear picture of

293 'placoderm' interrelationships.

294   *Minjinia turgenensis* reveals new data on 'placoderm' endoskeleton and tissue

295 diversity recorded from Mongolia—an otherwise extremely poorly known biogeographic

296 realm for early gnathostomes. The phylogenetic placement of this 'acanthothoracid'-like

297 taxon crownward of all non-maxillate 'placoderms', in conjunction with possession of

298 extensive endochondral bone, highlights the importance of material from traditionally

299 undersampled geographic areas. The presence of endochondral bone renews the hypothesis

300 that this tissue is evolutionarily ancient and was lost secondarily in chondrichthyans[6,33]. This

301   view is overall consistent with evidence of generalised bone loss in chondrichthyans,

302   potentially as a result of the suppression of bone-generating molecular genetic pathways[51,52].

303   Continued work in Mongolia and re-evaluation of phylogenetic datasets will be necessary to

304   address this, with the results likely to lead to substantial re-evaluation of gnathostome

305   phylogeny.

306

307

308   **Methods**

309

310   **X-ray computed microtomography.** We scanned MPC-FH100/9.1 using the Nikon XT

311   225s at the Museum of Paleontology, University of Michigan with the following parameters:

312   200kV, 140μA, over 3123 projections and a voxel size of 32.92μm. We conducted

313   segmentation using Mimics 19.0 (http://biomedical.materialise.com/mimics; Materialise,

314   Leuven, Belgium) and we imaged models for publication using Blender

315   (https://www.blender.org).

316   **Synchrotron light propagation phase contrast tomography.** We imaged *Diplacanthus*

317   *crassismus* specimen NMS 1891.92.334 on Beamline 19 of the European Synchrotron

318   Radiation Facility, using propagation phase-contrast synchrotron microtomography. We

319   performed a spot scan with an energy of 116keV, achieving a voxel size of 0.55 μm. We

320   processed the resulting tomograms using VG StudioMax 2.2 (Volume Graphics, Germany),

321   and prepared images in Blender.

322   **Phylogenetic analysis.** We conducted a parsimony analysis using TNT 1.5[54] and Bayesian

323   analysis using MrBayes v 3.2.7[55]. The dataset consisted of 95 taxa and 284 discrete

324   characters based on a pre-existing dataset[56]. We employed Osteostraci and Galeaspida as

325   composite outgroups. We conducted parsimony analysis using both equal weights and

326   implied weights methods. Global settings were 1000 search replicates and a hold of up to 1

327   million trees. Equal weights parsimony analyses were conducted using the ratchet with

328   default settings. Implied weights parsimony used a concavity parameter of 3 and the search

329   was without the ratchet. Command lists are included in Supplementary Information. We

330   conducted Bayesian analysis using both a partitioned and unpartitioned dataset. We used the

331   Mkv model[57] and gamma rate distribution. We ran the analyses for 5 million generations with

332   a relative burn-in fraction of 0.25. Runs were checked for convergence using Tracer[58]. We

333   partitioned the dataset using a newly proposed method[28] that partitions the data according to

334   homoplasy levels. Using the results of implied weights parsimony conducted in TNT, we

335   created a text table of character fit values. We wrote an R[59] script to generate a list of

336   partition commands for MrBayes.

337   We assessed parsimony ancestral states visually using Mesquite[60]. Likelihood and

338   Bayesian ancestral states were estimated in R using the castor package[61] version 1.5.7. Prior

339   to calculating likelihood ancestral states on parsimony trees, we scaled branch lengths using

340   PAUP*[62] and calculated the likelihood scores for all of the trees under the Mkv model with

341   gamma rate parameter. The trees were then exported with branch lengths. To account for

342   overall uncertainty in tree estimates, we estimated ancestral states on 100 trees randomly

343   selected from the fundamental set of most parsimonious trees and two times 50 trees selected

344   from the 75% last trees of each posterior tree distribution from the Bayesian analysis. We

345   then run an ancestral states estimation Mk model (using the castor R package) using both the

346   Equal Rates (ER) and All Rates Different (ARD) models. This resulted in 400 ancestral states

347   estimations. For each estimation we extracted the overlap log likelihood, the AIC (counting

348   one parameter for the ER model and two for the ARD model) and the scaled log likelihood

349   (probability) for the presence and absence of the endochondral bone character (character 4)

350   for the last common node of *Minjinia* and crown-group gnathostomes. We present the median

351 value of these distributions of the estimations overall log likelihoods, AICs and presence or

352 absence of endochondral bone in Table 1.

353

354 **Data availability**

355 The holotype specimen of *Minjinia turgenensis* will be permanently deposited in the

356 collections of the Institute of Paleontology, Mongolian Academy of Sciences. Original

357 tomograms are available at (doi:10.6084/m9.figshare.12301229) and rendered models are

358 available at (doi:10.6084/m9.figshare.12301223). The phylogenetic character list and dataset

359 are available as Supplementary Information S1 and S2. The LifeScience Identifier for

360 *Minjinia turgenensis* is urn:lsid:zoobank.org:act:82A1CEEC-B990-47FF-927A-

361 D2F0B59AEA87

362

363 **Code availability**

364 R code for generating partitions based on character fits and code for likelihood ancestral

365 states reconstructions and plots are available in the Supplementary Information.

366

367 **References**

368 1.   Hall, B. K. *Bones and Cartilage*. (Academic Press, 2005).

369 2.   Janvier, P. *Early Vertebrates*. (Oxford University Press, 1996).

370 3.   Donoghue, P. C. J., Sansom, I. & Downs, J. P. Early evolution of vertebrate skeletal

371   tissues and cellular interactions, and the canalization of skeletal development. *Journal*

372   *of Experimental Zoology* **306B,** 278–294 (2006).

373 4.   Rosen, D. E., Forey, P. L., Gardiner, B. G. & Patterson, C. Lungfishes, tetrapods,

374   paleontology, and plesiomorphy. *Bull Am Mus Nat Hist* **167,** 159–276 (1981).

375   5.   Gardiner, B. G. The relationships of the palaeoniscid fishes, a review based on new

376   specimens of *Mimia* and *Moythomasia* from Upper Devonian of Western Australia.

377   *Bull Br Mus nat Hist (Geol)* **37,** 173–428 (1984).

378   6.   Maisey, J. G. Heads and tails: a chordate phylogeny. *Cladistics* **2,** 201–256 (1986).

379   7.   Friedman, M. & Brazeau, M. A Reappraisal of the origin and basal radiation of the

380   Osteichthyes. *J Vertebr Paleontol* **30,** 36–56 (2010).

381   8.   Maisey, J. G., Denton, J. S. S., Burrow, C. & Pradel, A. Architectural and

382   ultrastructural features of tessellated calcified cartilage in modern and extinct

383   chondrichthyan fishes. *Journal of Fish Biology* **15,** 37–23 (2020).

384   9.   Karatajūtė-Talimaa, V. & Novitskaya, L. *Sodolepis*—a new representative of

385   Mongolepidida (Chondrichthyes?) from the lower Silurian of Mongolia.

386   *Paleontologicheskii Zhurnal* **5,** 96–103 (1997).

387   10.   Karatajūtė-Talimaa, V. & Novitskaya, L. *Teslepis*—a new representative of

388   mongolepid elasmobranchs from the Lower Silurian of Mongolia. *Paleontologicheskii*

389   *Zhurnal* **4,** 36–43 (1992).

390   11.   Karatajūtė-Talimaa, V., Novitskaya, L. & Rozman, K. S. *Mongolepis*—a new lower

391   Silurian genus of elasmobranchs from Mongolia. *Paleontologicheskii Zhurnal* **1,** 76–

392   86 (1990).

393   12.   Andreev, P. *et al.* The systematics of the Mongolepidida (Chondrichthyes) and the

394   Ordovician origins of the clade. *PeerJ* **4,** e1850–e1850 (2016).

395   13.   Vorobjeva, E. I. & Janvier, P. Observations to the note by E Vorobjeva: 'First

396   discovery of Palaeozoic fishes on the territory of the Mongolian Republic'.

397   *Palaeontology and Biostratigraphy of Mongolia*, Moscow, 3, 134-136 (in Russian).

398   *Geobios* **17,** 379–380 (1984).

399   14.   Gegenbaur, C. *Grundriss der vergleichenden Anatomie*. 1–680 (Wilhelm Engelmann,

400   1874).

401   15.   Alekseeva, R. E., Mendbayar, B. & Erlanger, O. A. *Brachiopods and Biostratigraphy*

402   *of the Lower Devonian of Mongolia*. **16,** (Nauka, 1981).

403   16.   Alekseeva, R. E. *Devonian Biostratigraphy of Mongolia*. (Nauka, 1993).

404   17.   Mark-Kurik, E. in *Morphology, Phylogeny and Paleobiogeography of Fossil Fishes*

405   (eds. Elliott, D. K., Maisey, J., Yu, X. & Miao, D.) 101–106 (2010).

406   18.   Ørvig, T. Description, with special reference to the dermal skeleton, of a new radotinid

407   arthrodire from the Gedinnian of Arctic Canada. *Colloque international C.N.R.S. no.*

408   *218* 43–71 (1975).

409   19.   Olive, S., Goujet, D., Lelièvre, H. & Janjou, D. A new Placoderm fish

410   (Acanthothoraci) from the Early Devonian Jauf Formation (Saudi Arabia).

411   *Geodiversitas* **33,** 393–409 (2011).

412   20.   Wängsjö, G. The Downtonian and Devonian vertebrates of Spitsbergen. IX. *Norsk*

413   *Polarinstitutt Skrifter* **97,** 1–611 (1952).

414   21.   Charest, F., Johanson, Z. & Cloutier, R. Loss in the making: absence of pelvic fins and

415   presence of paedomorphic pelvic girdles in a Late Devonian antiarch placoderm

416   (jawed stem-gnathostome). *Biology Letters* **14,** 20180199 (2018).

417   22.   Dupret, V., Sanchez, S., Goujet, D. & Ahlberg, P. E. The internal cranial anatomy of

418   *Romundina stellina* Ørvig, 1975 (Vertebrata, Placodermi, Acanthothoraci) and the

419   origin of jawed vertebrates—Anatomical atlas of a primitive gnathostome. *PLoS ONE*

420   **12,** e0171241 (2017).

421   23.   Stensiö, E. A. La cavité labyrinthique, l'ossification sclérotique et l'orbite de *Jagorina*.

422   *Colloques internationaux du Centre national de la Recherche scientifique* **21,** 9–43

423   (1950).

424   24.   Stensiö, E. A. Anatomical studies on the arthrodiran head. *K Sven Vetenskapsakad*

425   *Handl* **9,** 1–419 (1963).

426   25.   Goujet, D. *Les poissons placodermes du Spitsberg*. (Cahiers de Paléontologie, Editions

427   du CNRS, 1984).

428   26.   Davis, S. P., Finarelli, J. A. & Coates, M. I. *Acanthodes* and shark-like conditions in

429   the last common ancestor of modern gnathostomes. *Nature* **486,** 247–250 (2012).

430   27.   Castiello, M. & Brazeau, M. D. Neurocranial anatomy of the petalichthyid placoderm

431   *Shearsbyaspis oepiki* Young revealed by X-ray computed microtomography.

432   *Palaeontology* **61,** 369–389 (2018).

433   28.   Rosa, B. B., Melo, G. A. R. & Barbeitos, M. S. Homoplasy-based partitioning

434   outperforms alternatives in Bayesian analysis of discrete morphological data.

435   *Systematic Biology* **54,** 373 (2019).

436   29.   Brazeau, M. D. & Friedman, M. The characters of Palaeozoic jawed vertebrates. *Zool*

437   *J Linn Soc* **170,** 779–821 (2014).

438   30.   Zhu, M. *et al.* A Silurian placoderm with osteichthyan-like marginal jaw bones. *Nature*

439   **502,** 188–193 (2013).

440   31.   Giles, S., Friedman, M. & Brazeau, M. D. Osteichthyan-like cranial conditions in an

441   Early Devonian stem gnathostome. *Nature* **520,** 82–85 (2015).

442   32.   Miles, R. S. in *Interrelationships of Fishes* (eds. Greenwood, P. H., Miles, R. S. &

443   Patterson, C.) 63–103 (Academic Press London, 1973).

444   33.   Zhu, M. Bone gain and loss: insights from genomes and fossils. *Natl Sci Rev* **1,** 490–

445   492 (2014).

446   34.   Janvier, P. *Les céphalaspides du Spitsberg*. (Éditions du Centre National de la

447   Recherche Scientifique, 1985).

448 35. Ørvig, T. Histologic studies of placoderms and fossil elasmobranchs. *Arkiv för Zoologi*

449 **2,** 321–454 (1951).

450 36. Young, G. C. New information on the structure and relationships of *Buchanosteus*

451 (Placodermi: Euarthrodira) from the Early Devonian of New South Wales. *Zool J Linn*

452 *Soc* **66,** 309–352 (1979).

453 37. Miles, R. S. & Young, G. C. in *Problems in Vertebrate Evolution* (eds. Andrews, S.

454 M., Miles, R. S. & Walker, A. D.) 123–198 (Academic Press, 1977).

455 38. Stensiö, E. A. On the head of the macropetalichthyids. *Field Museum of Natural*

456 *History Publication Geological Series* **4,** 87–197 (1925).

457 39. Ørvig, T. Notes on some Paleozoic lower vertebrates from Spitsbergen and North

458 America. *Norsk Geologisk Tidsskrift* **37,** 285–353 (1957).

459 40. Sansom, R. Phylogeny, classification and character polarity of the Osteostraci

460 (Vertebrata). *Journal of Systematic Palaeontology* **7,** 95–115 (2009).

461 41. Schaeffer, B. The braincase of the holostean fish *Macrepistius*, with comments on

462 neurocranial ossification in the Actinopterygii. *American Museum Novitates* **2459,** 1–

463 34 (1971).

464 42. Watson, D. M. S. The acanthodian fishes. *Philosophical Transactions of the Royal*

465 *Society of London. Series B, Biological Sciences* **228,** 49–146 (1937).

466 43. Burrow, C. J., Davidson, R. G., Blaauwen, den, J. L. & Newman, M. J. Revision of

467 *Climatius reticulatus* Agassiz, 1844 (Acanthodii, Climatiidae), from the Lower

468 Devonian of Scotland, based on new histological and morphological data. *J Vertebr*

469 *Paleontol* **35,** e913421 (2015).

470 44. Dean, M. N., Socha, J. J., Hall, B. K. & Summers, A. P. Canaliculi in the tessellated

471 skeleton of cartilaginous fishes. *Journal of Applied Ichthyology* **26,** 263–267 (2010).

472   45.   Atake, O. J., Cooper, D. M. L. & Eames, B. F. Bone-like features in skate suggest a

473   novel elasmobranch synapomorphy and deep homology of trabecular mineralization

474   patterns. *Acta Biomaterialia* **84,** 424–436 (2019).

475   46.   Pearson, D. M. & Westoll, T. S. The Devonian actinopterygian *Cheirolepis* Agassiz.

476   *Transactions of the Royal Society of Edinburgh: Earth Sciences* **70,** 337–399 (1979).

477   47.   Giles, S. *et al.* Endoskeletal structure in *Cheirolepis* (Osteichthyes, Actinopterygii), An

478   early ray-finned fish. *Palaeontology* **58,** 849–870 (2015).

479   48.   Grande, L. & Bemis, W. E. Osteology and Phylogenetic Relationships of Fossil and

480   Recent Paddlefishes (Polyodontidae) with Comments on the Interrelationships of

481   Acipenseriformes. *Memoir (Society of Vertebrate Paleontology)* **11 (Supplement to**

482   **Number 1),** 1–121 (1991).

483   49.   Eames, B. F. *et al.* Skeletogenesis in the swell shark *Cephaloscyllium ventriosum.*

484   *Journal of Anatomy* **210,** 542–554 (2007).

485   50.   Venkatesh, B. *et al.* Elephant shark genome provides unique insights into gnathostome

486   evolution. *Nature* **505,** 174–179 (2014).

487   51.   Ryll, B., Sanchez, S., Haitina, T., Tafforeau, P. & Ahlberg, P. E. The genome of

488   *Callorhinchus* and the fossil record: a new perspective on SCPP gene evolution in

489   gnathostomes. *Evolution & Development* **16,** 123–124 (2014).

490   52.   Marconi, A., Hancock-Ronemus, A. & Gillis, J. A. Adult chondrogenesis and

491   spontaneous cartilage repair in the skate, *Leucoraja erinacea. eLife Sciences* **9,** 2813

492   (2020).

493   53.   King, B., Qiao, T., Lee, M. S. Y., Zhu, M. & Long, J. A. Bayesian morphological

494   clock methods resurrect placoderm monophyly and reveal rapid early evolution in

495   jawed vertebrates. *Systematic Biology* **66,** 499–516 (2016).

496   54.   Goloboff, P. A. & Catalano, S. A. TNT version 1.5, including a full implementation of

497   phylogenetic morphometrics. *Cladistics* **32,** 221–238 (2016).

498   55.   Ronquist, F. & Huelsenbeck, J. P. MrBayes 3: Bayesian phylogenetic inference under

499   mixed models. *Bioinformatics* **19,** 1572–1574 (2003).

500   56.   Clement, A. M. *et al.* Neurocranial anatomy of an enigmatic Early Devonian fish sheds

501   light on early osteichthyan evolution. *eLife Sciences* **7,** e34349 (2018).

502   57.   Lewis, P. O. A likelihood approach to estimating phylogeny from discrete

503   morphological character data. *Systematic Biology* **50,** 913 (2001).

504   58.   Rambaut, A., Drummond, A. J., Xie, D., Baele, G. & Suchard, M. A. Posterior

505   summarization in Bayesian phylogenetics using Tracer 1.7. *Systematic Biology* **67,**

506   901–904 (2018).

507   59.   R Core Team. *R: A language and environment for statistical computing.* (R

508   Foundation for Statistical Computing, 2019).

509   60.   Maddison, D. R. & Maddison, W. P. *Mesquite.* (2019).

510   61.   Louca, S. & Doebeli, M. Efficient comparative phylogenetics on large trees.

511   *Bioinformatics* **34,** 1053–1055 (2017).

512   62.   Swofford, D. L. *PAUP*.* 4.0a166, (2019).

513

531

532   **Author Contributions:** MDB conceived and designed the study. MDB, AJ, YAA, and EZ

533   participated in all field seasons. RPD and AJ undertook preliminary CT scanning and

534   segmentation that revealed the fossil was a 'placoderm' and had endochondral bone. RS

535   discovered the first vertebrate remains in the first field season at Yamaat Gol in 2010. SG

536   undertook the segmentation of *Minjinia* with input from MDB. AJ performed segmentation

537   of *Diplacanthus* tissue. MC provided input on occipital comparative morphology of

538   'placoderms'. RPD provided data and comparative analyses and data for endoskeletal tissue.

539   YAA provided background on the geology, palaeontology, and stratigraphy of the type

540   location; EZ and YAA organized field logistics and permitting. MDB, SG, MC, RPD, and AJ

541   undertook the anatomical interpretation and prepared the figures. MDB and SG conducted the

542   phylogenetic analyses. RS conducted the parsimony branch support analyses. TG wrote the

543   script for generating MrBayes partitions from TNT's character fits table and conducted the

544   likelihood and model-fitting analyses. The manuscript was written by MDB, RPD, and SG.

545

546 **Competing interests statement:**
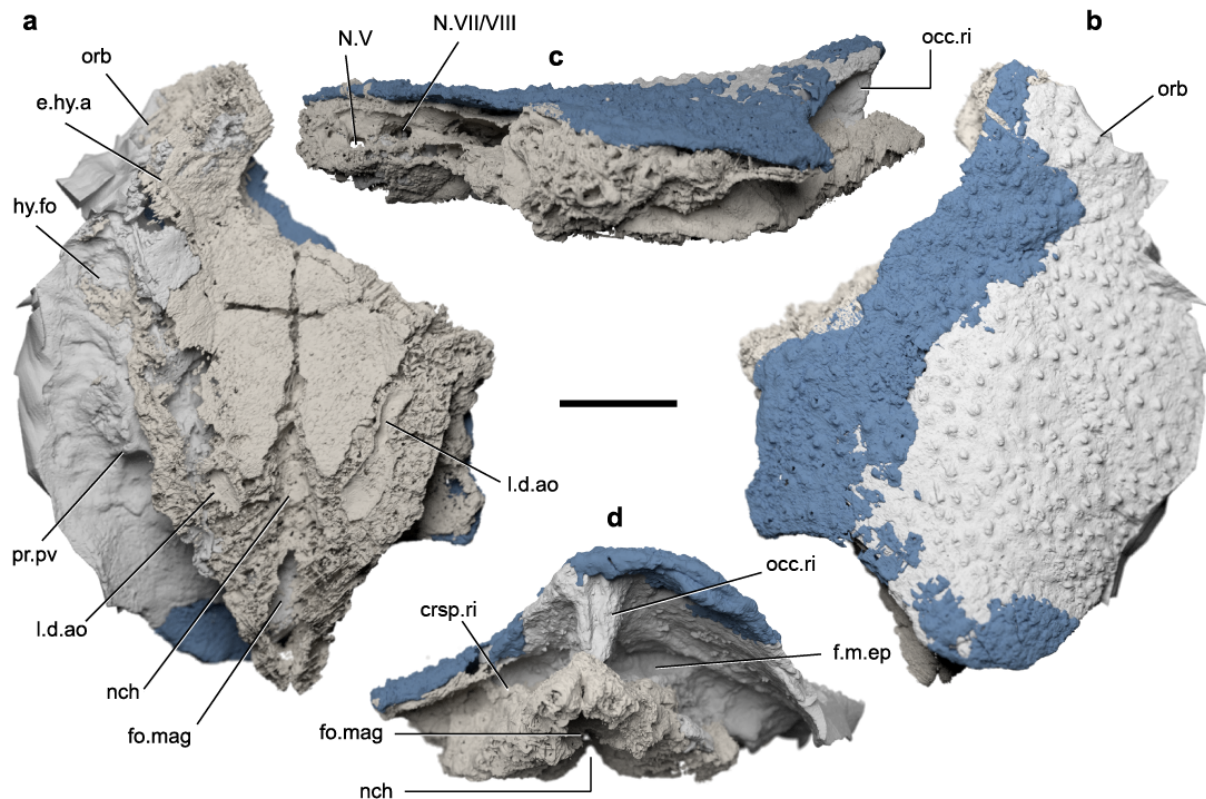
547 The authors declare no competing interests.

Fig. 1 | MPC-FH100/9.1 a 'placoderm' skull roof and braincase from the Early Devonian of Mongolia. a, Ventral view. **b**, Dorsal view. **c**, Left lateral view. **d**, Posterior view. **e**, Braincase endocavity in dorsal view. Taupe: endoskeleton; grey: mould; blue: exoskeleton. crsp.ri, craniospinal ridge; e.hy.a, sulcus for the efferent hyoid artery; f.m.ep, epaxial muscle fossa; fo.mag., foramen magnum; hy.fo, hyodean fossa; l.d.ao, sulcus for the lateral dorsal aorta; N.V, trigeminal nerve canal; N.VII, facial nerve canal; N.VIII, acoustic nerve canal; nch, notochordal canal; occ.ri, occipital ridge; orb, orbit; pr.pv, paravagal process. Scale bar, 10 mm.
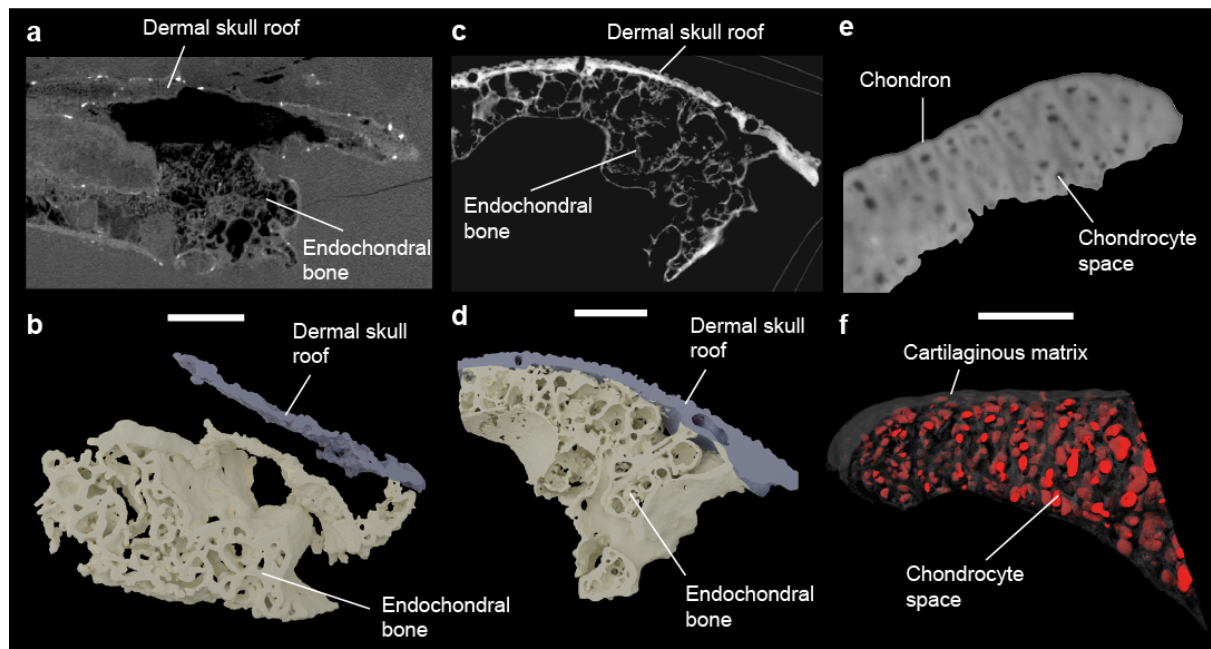
Fig. 2 | Endoskeletal mineralisation in fossil gnathostomes. a, Transverse tomographic slice through MPC-FH100/9.1. **b**, Three-dimensional rendering of trabecular bone structure. **c**, Transverse tomographic section through the braincase of the osteichthyan *Ligulalepis*. **d**, Three-dimensional rendering of the trabecular bone in *Ligulalepis* (**c** and **d** use data from[56]). **e**, Synchrotron tomography image of the calcified cartilage of the certatohyal of the stem-group chondrichthyan *Diplacanthus crassisimus* specimen NMS 1891.92.334. **f**, Semi-transparent three-dimensional structure of calcified cartilage of NMS 1891.92.334. Scale bars, **a** and **b,** 10 mm; **c** and **d**, 1 mm; **e** and **f**, 150 μm.
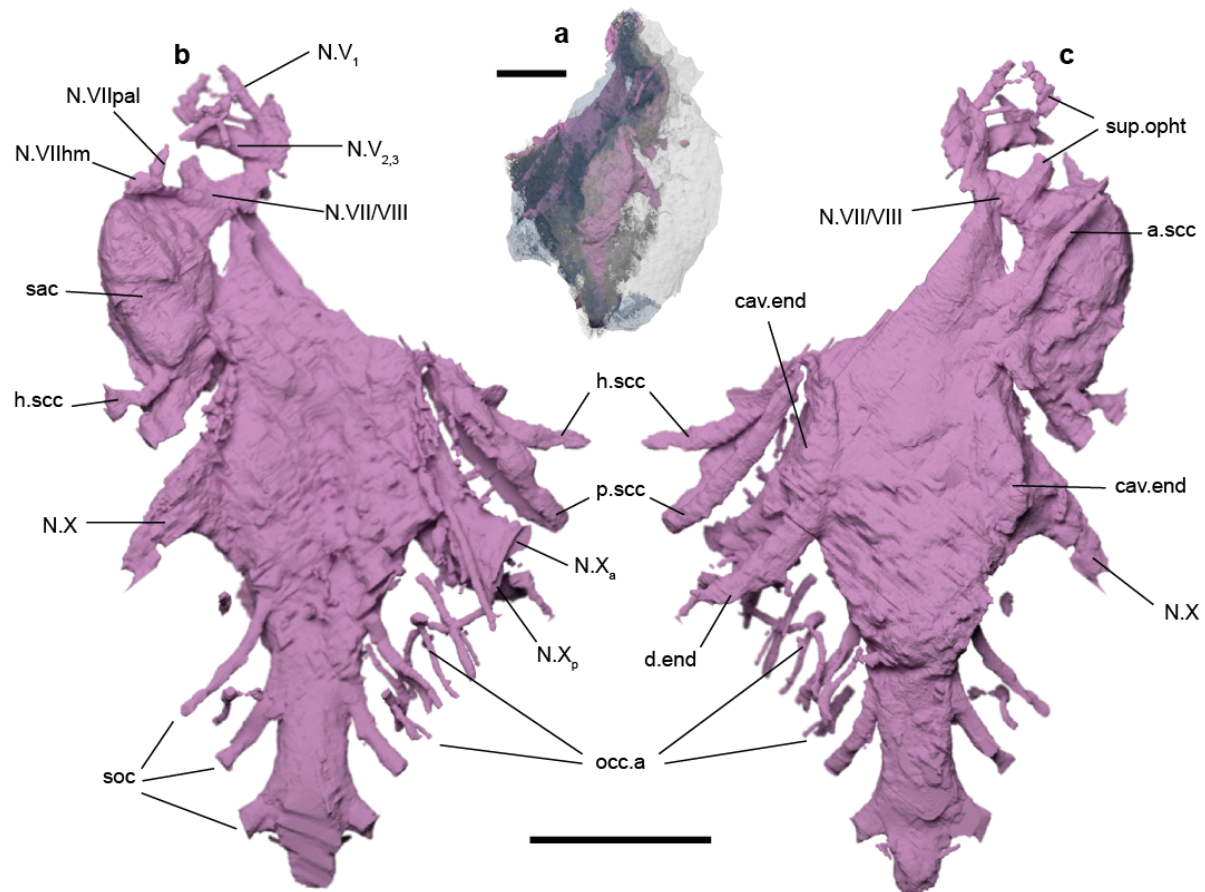
Fig. 3 | Braincase endocavity of *Minjinia*. a, Semi-transparent rendering of skull roof and braincase (grey and blue) showing extent of endocavity (pink). **b,** Ventral view. **c,** Dorsal view. a.scc, anterior semicircular canal; cav.end, endolymphatic cavity; d.end, endolymphatic duct; h.scc, horizontal semicicular canal; N.V, trigeminal nerve canal; N.VIIhm, hyomandibular branch of facial nerve canal; N.VIIpal, palatine branch of facial nerve canal; N.VIII, acoustic nerve canal; N.X, vagus nerve canal, N.X$_a$, anterior branch of vagus nerve canal; N.X$_p$, posterior branch of vagus nerve canal; occ.a, occipital artery canals; p.scc, posterior semicircular canal; sac, sacculus; soc, spino-occipital nerve canals; sup.opth, canal for supra-ophtalmic nerve. Scale bars, 10 mm (upper scale bar associates with **a**, lower scale bar associates with **b** and **c**).
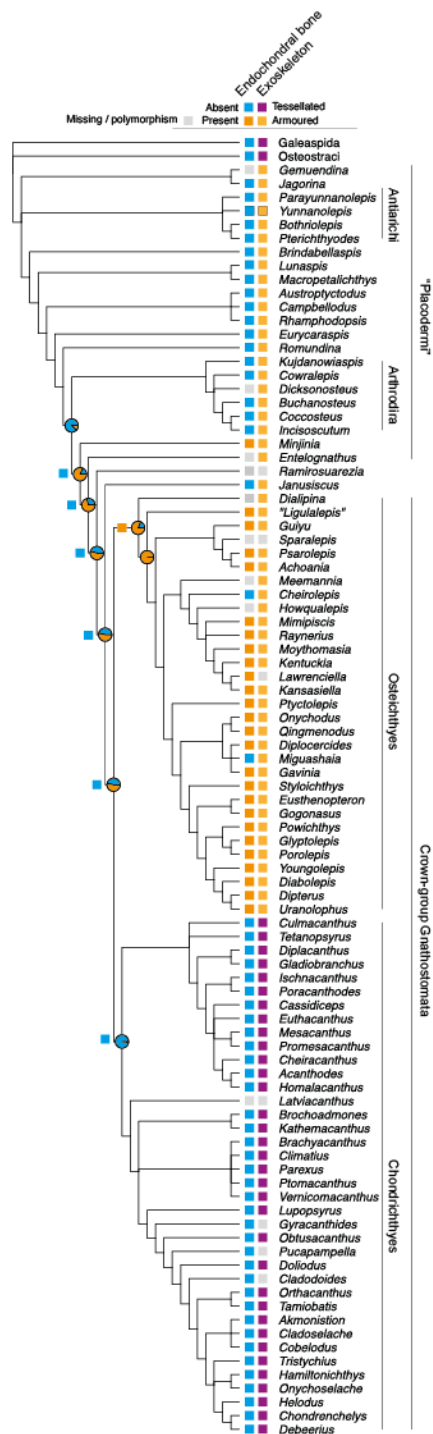
Fig. 4 | Strinct consensus tree from parsimony analysis of early gnathostomes showing

distribution of endochondral bone and exoskeletal armour. Squares at nodes indicate

parsimony reconstruction for endochondral bone. Pie charts at nodes show likelihood

reconstructions for the same character under the all-rates-different model (see Extended Data

Figs 6 & 7 for competing reconstructions). Grey box indicates uncertainty. Loss of

586   endochondral bone maps closely with generalised loss of bone in chondrichthyans where

587   exoskeletal armour and perichondral bone are also absent.

588

589   **Table 1 | Tree distribution (n=100) ancestral states estimation results.** ER = Equal rates

590   model; ARD = All Rates Different model. The columns AIC and log.like represent the

591   median AIC and log.lik across the 100 parsimony and Bayesian trees (for both models). The

592   like.ratio column is the likelihood ratio for the models compared on these trees. The columns

593   Absent and Present represent the median scaled likelihood for the endochondral bone state.

trees	model	log.like.	like.ratio	AIC	node	Absent	Present
Parsimony	ER	-28.91	4.74	59.82	Minjinia:Gnathostomes	0.67	0.33
(equal weights)	ARD	-26.54		57.09		0.19	0.81
	ER				Crown Gnathostomes	0.91	0.09
	ARD					0.46	0.54
Bayesian	ER	-29.66	5.26	61.32	Minjinia:Gnathostomes	0.73	0.27
(unpartitioned)	ARD	-27.03		58.06		0.17	0.83
	ER				Crown Gnathostomes	0.79	0.21
	ARD					0.22	0.78

594

595
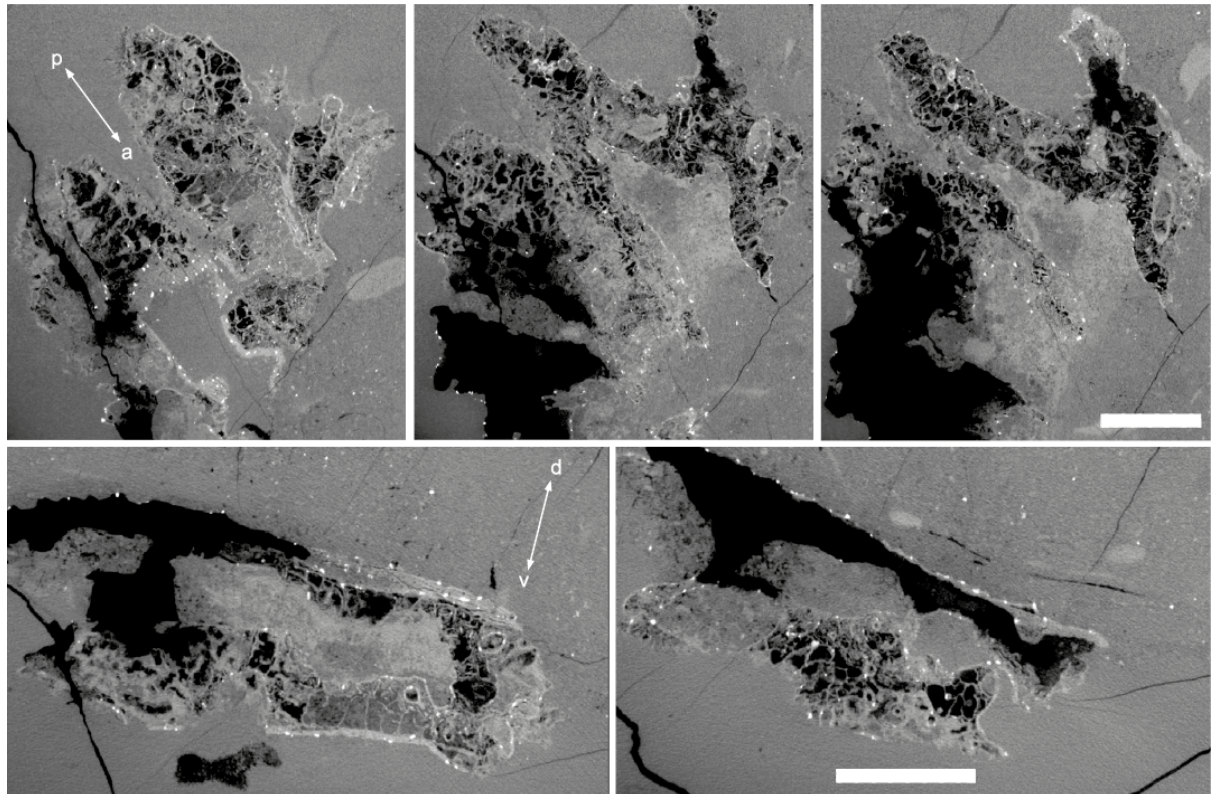
Extended Data Fig. 1 | Tomograms of endoskeletal ossification in *Minjinia*. Top row:

semi-coronal sections through braincase. Double-headed arrows indicate anterior-posterior

(a-p) dorsal-ventral (d-v) axes. Bottom row: semi-transverse sections through posterior part

of endocranium. Voids of black space represent mouldic preservation. Scale bars, 10 mm and

apply across each row of panels.

601
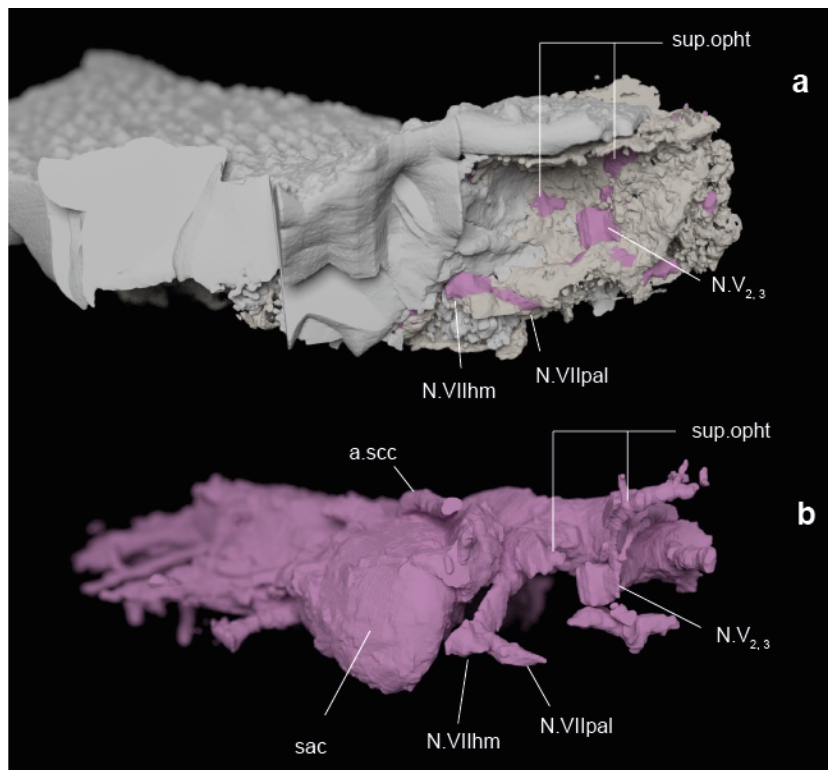
Extended Data Fig. 2 | Right orbital wall and innervation pattern of *Minjinia*. a, orbit in anterolateral view showing disposition of nerve openings (pink infill). **b**, endocast in the same perspective showing the relationship between nerve canals and endocast. a.scc., anterior semicircular canal; $N.V_{2,3}$ trunk of the trigeminal nerve canal for branches 2 and 3; N.VIIhm, hyomandibular branch of facial nerve canal; N.VIIpal, palatine branch of facial nerve canal; sac., sacculus; sup.opth, canal for supra-ophtalmic nerve. Scale bars, 20 mm (upper scale bar associates with **a**, lower scale bar associates with **b** and **c**).

611
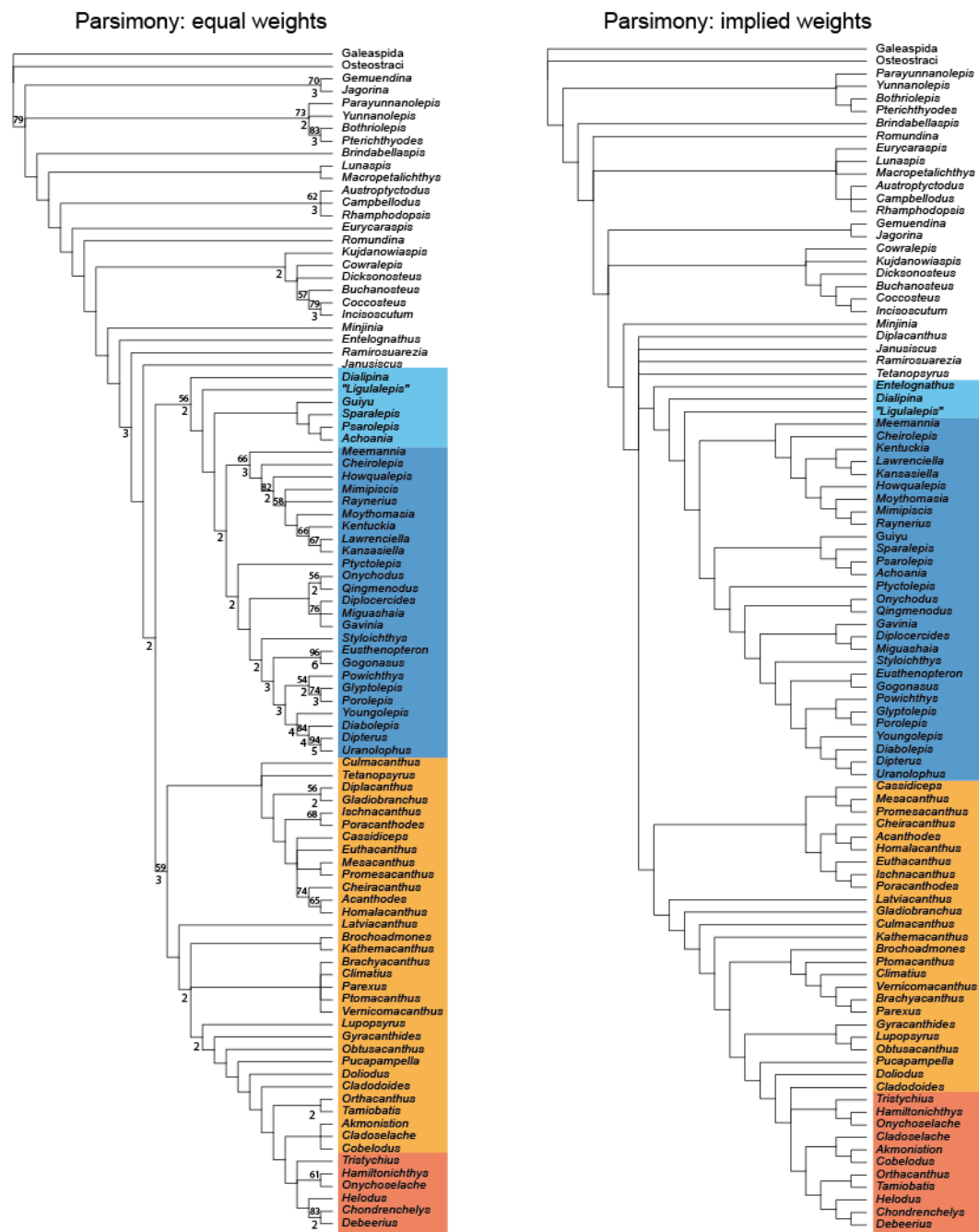
Extended Data Fig. 3 | Results of phylogenetic parsimony analysis. Dataset consists of 95

taxa and 284 characters. Both trees are strict consensus topologies. Equal weights parsimony

analysis using the ratchet resulted in 240 trees with a length of 831 steps. Implied weights

parsimony analysis using random addition sequence + branch-swapping resulted in 8 optimal

trees with score 85.20513. Double-digit figures above internal branches are bootstrap values

of 50% and over; single-digit figures below branches are Bremer decay index values. Blue

shading: osteichthyan total group (dark blue: crown group); orange shading: chondrichthyan

total group (dark orange: crown group).
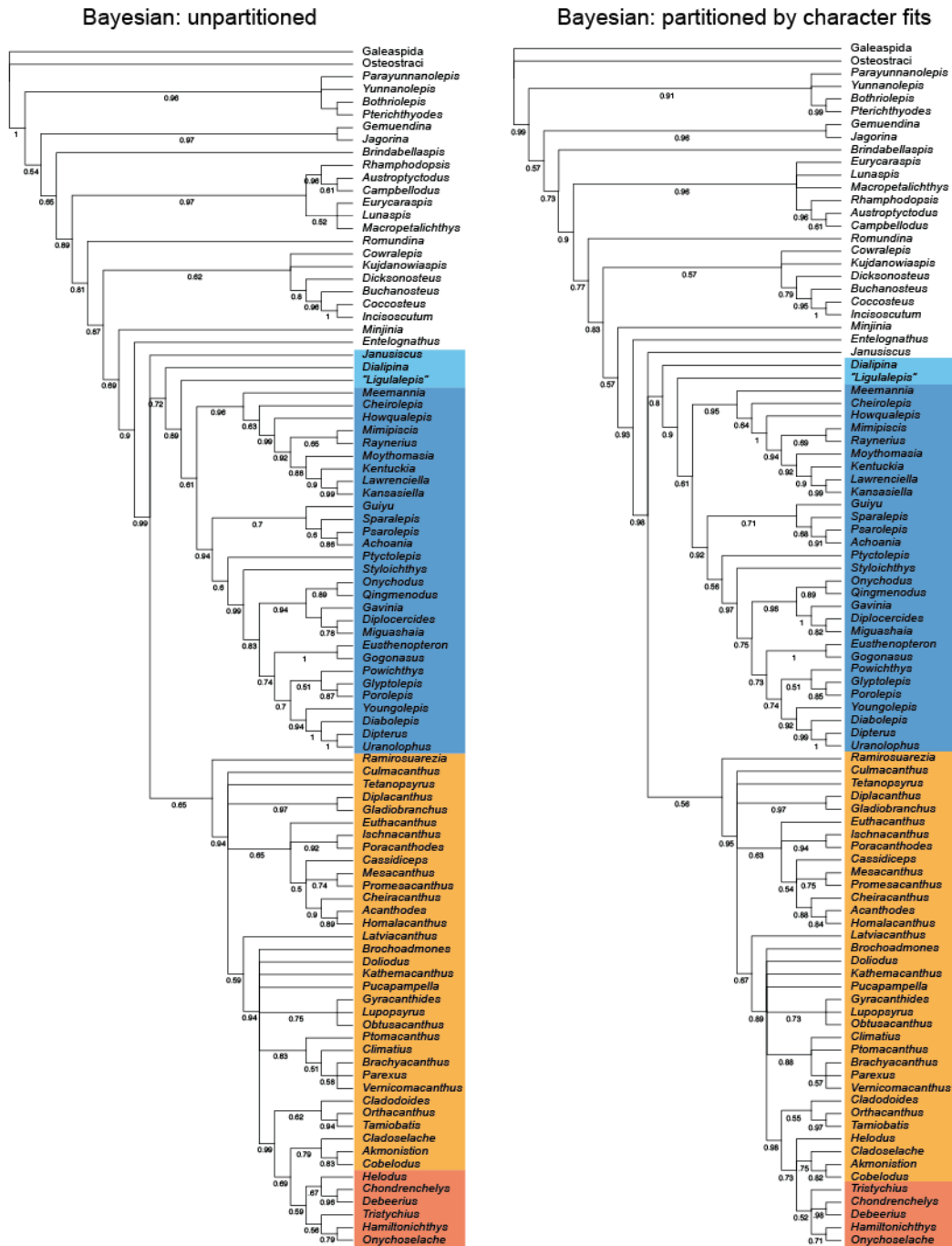
**Extended Data Fig. 4 | Results of Bayesian phylogenetic analysis using both partitioned and unpartitioned data.** Majority-rules consensus trees with posterior probabilities shown

624   along branches. Blue shading: osteichthyan total group (dark blue: crown group); orange

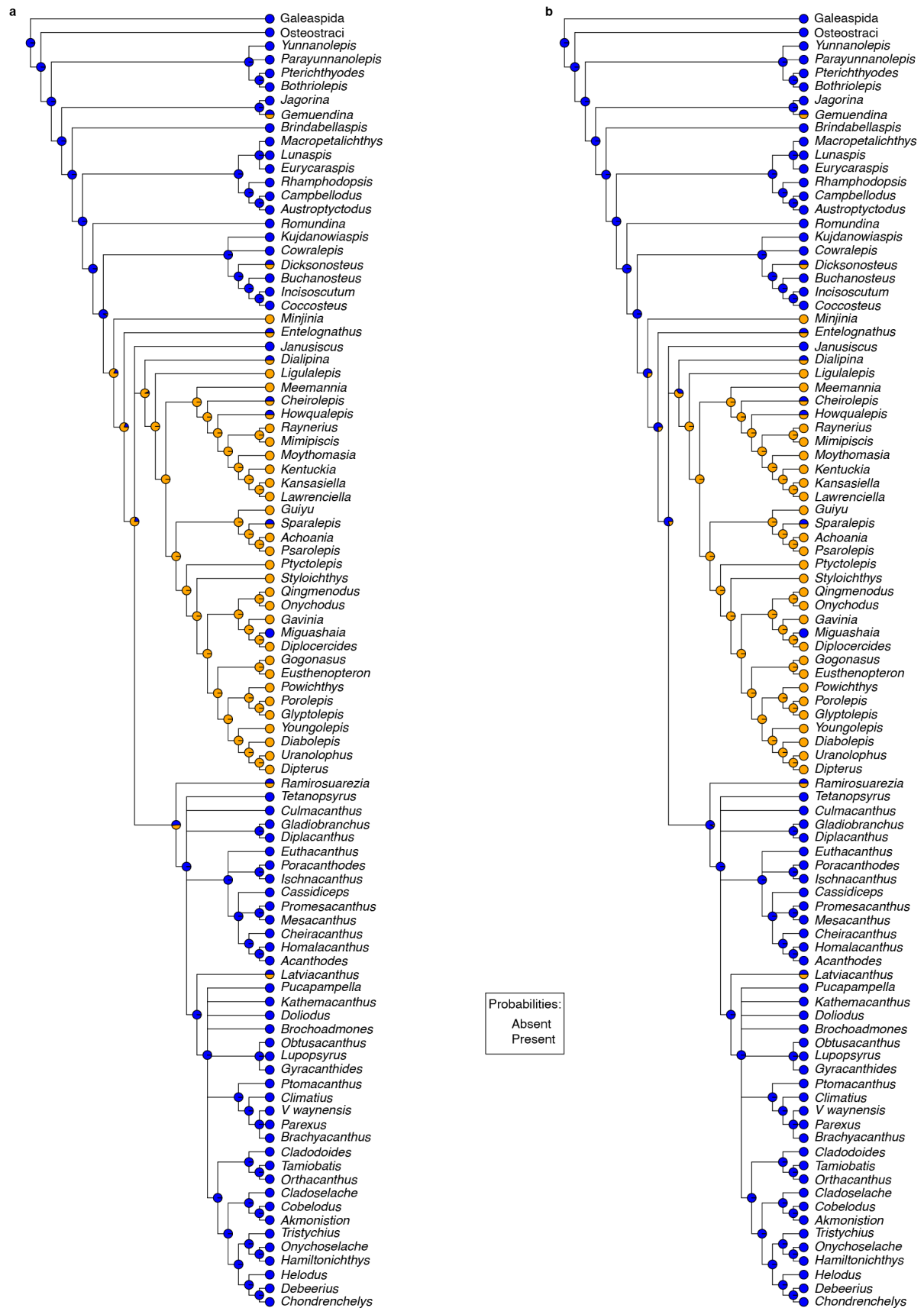625   shading: chondrichthyan total group (dark orange: crown group).

626

627

Extended Data Fig. 5 | Likelihood ancestral state mapping of endochondral bone on
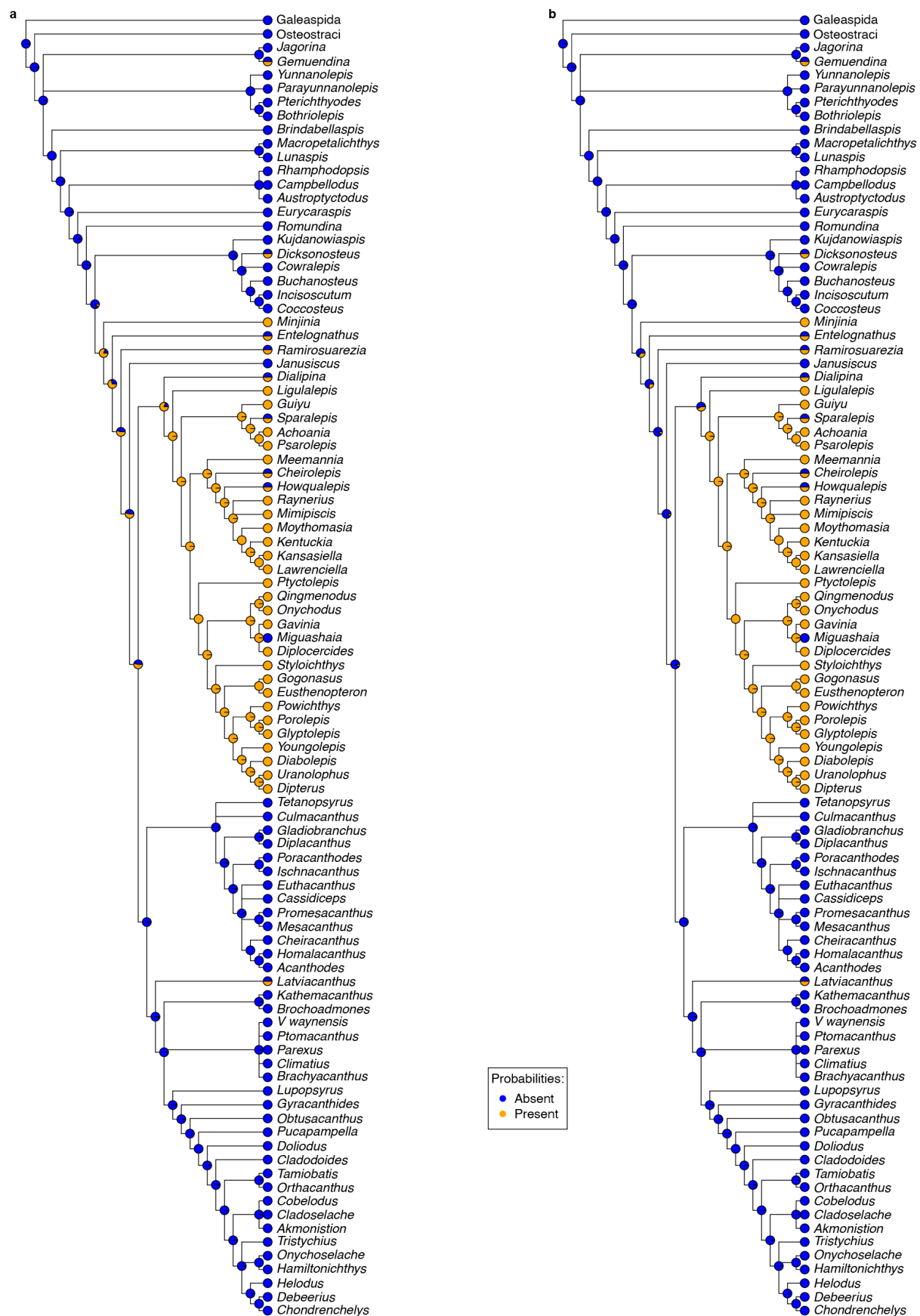
629   **equal weights parsimony results. a**, ARD, all rates different model; **b**, ER, equal rates

630   model.

631

632

Extended Data Fig. 6 | Likelihood ancestral state mapping of endochondral bone on

634   **unpartitioned Bayesian analysis results. a**, ARD, all rates different model; **b**, ER, equal

635   rates model.